IEEE Journal of Microwaves

Received 7 June 2022; revised 29 July 2022; accepted 24 August 2022. Date of publication 15 September 2022; date of current version 7 October 2022.

Digital Object Identifier 10.1109/JMW.2022.3202162

Dual-Narrowband/Wideband Filters Using Modified Coaxial Cavities With Large Frequency Ratios

ZHI-CHONG ZHANG [1] (Member, IEEE), HONG-JI LI [2], XU-ZHOU YU [2] (Student Member, IEEE), YEJUN HE [2] (Senior Member, IEEE), AND SAI-WAI WONG [2] (Senior Member, IEEE)

(Regular Paper)

[1]College of Electronic and Information Engineering, Jinggangshan University, Ji'an 343009, China
[2]College of Information Engineering, Shenzhen University, Shenzhen 518060, China

CORRESPONDING AUTHOR: Sai-Wai Wong (e-mail: wongsaiwai@ieee.org).

This work was supported in part by the National Natural Science Foundation of China under Grants 61861022 and 62171289, in part by the Shenzhen Science and Technology Programs under Grant JCYJ 20190728151457763, in part by the Natural Science Foundation of Jiangxi, China under Grants 20192BAB217002 and 20212BCJL23062, and in part by the Science and Technology Project of Jiangxi Province Education Department under Grant GJJ201012.

ABSTRACT This article presents two types of dual-narrowband/ wideband filters using modified coaxial cavities with large frequency ratios. The dual-narrowband/ wideband filters mean two dual-band bandpass filters, one of which is a dual-band wideband filter, and the other is a dual-band narrowband filter. The proposed coaxial resonator in the dual-narrowband filter consists of a pair of disk-loaded coaxial stepped impedance resonator (DLCSIR), which provides a large frequency ratio. The frequency ratio of the first two resonant modes of the DLCSIR can be precisely controlled by adjusting the impedance ratios and dimensions of the loading disk. By contrast, the proposed coaxial resonator in the dual-wideband filter is a rectangular coaxial stepped impedance resonator (RCSIR), which has the merits of miniaturized size, large frequency ratio, and convenience for strong coupling. Finally, two second-order dual-narrowband/ wideband filters with large frequency ratios were designed, fabricated, and measured. The exhibited dual-passband performance of the two filters verifies the proposed concept.

INDEX TERMS Dual-band filter, large frequency ratio, disk loaded coaxial stepped impedance resonator (DLCSIR), rectangular coaxial stepped impedance resonator (RCSIR).

I. INTRODUCTION

Now, modern wireless communications systems are heading for high-speed data transmission. However, the frequency spectrum is getting crowded below 6 GHz, and the fifth-generation (5G) wireless systems have been moved up to the millimeter-wave spectrum, which triggers the demand for multiband filters with large frequency ratios, especially multi-wideband filters. Recently, dual-band planar filters with a large frequency ratio based on the complementary frequency response characteristics of the stepped-impedance resonator bandpass filter and low-pass filter [1] and mode composite coplanar waveguide [2] have been proposed. In addition, a tunable dual-band filter with a large frequency ratio, combining a microstrip bandpass filter and a dielectric-loaded bandpass filter, has been proposed in [3]. However, these structures are difficult to apply to the base transceiver stations. By contrast, multiband cavity filters can be broadly classified as dielectric-loaded filters [4], [5], [6], [7], helical filters [8], waveguide filters [9], [10], [11], [12], [13], [14], [15], and coaxial filters [16], [17], [18], [19], [20], [21], [22]. Despite the size advantage of dielectric-loaded filters, the closer harmonics make it more difficult to achieve large frequency ratios. Compared to significant insertion loss helical cavity filters and large-size waveguide cavity filters, coaxial cavity filters are more suitable for achieving large frequency ratio characteristics due to their use of quarter wavelength resonators, which are naturally far harmonics.

In this paper, DLCSIR is used to realize a dual-narrowband filter with a large frequency ratio, and RCSIR is employed to achieve a dual-wideband filter with a large frequency ratio for

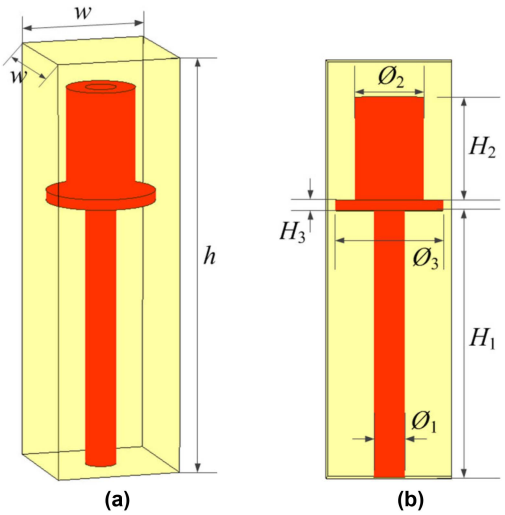

FIGURE 1. Proposed DLCSIR. (a) Three-dimensional view. (b) Front view.

the first time. There are two innovations in this paper. The first innovation is to achieve controllable resonant frequency by adding a disk on the coaxial stepped impedance resonator and achieving a controllable coupling coefficient through different magnetic fields of the fundamental and second modes. The second innovation is to achieve a strong coupling through rectangular step transmission lines across the coupling window, thus realizing a dual-wideband filter. The dual-narrowband filter has resonators with a large frequency ratio and an adaptive feeding structure and coupling structure, which provides independently controlled frequencies and bandwidths of the two bands in a specific range. Moreover, the dual-wideband filter adopts a resonant structure which is easy to realize strong coupling. Meanwhile, miniaturized size is also one of its characteristics. A detailed analysis of the two novel filters is introduced, including resonator analysis, feeding analysis, coupling analysis, and filter design. Finally, two examples of the proposed second-order dual-narrowband/ wideband filters are demonstrated. This paper is organized as follows. A detailed design analysis of the dual-narrowband filter and dual-wideband filter is provided in Section II and Section III, respectively. Finally, Section IV is the conclusion of this paper, and the whole design is summarized.

II. DUAL-NARROWBAND FILTER DESIGN

A. DLCSIR ANALYSIS

The geometry of DLCSIR is depicted in Fig. 1. This resonator is formed on a cuboid cavity with the length and width both are parameter w, and the height is parameter h. A disk-loaded stepped impedance coaxial line is embedded vertically in the center of the bottom sidewall of the cavity. The specific parameters are shown in Fig. 1(b). The fundamental and second modes are used to achieve the two narrow passbands of the filter.

CST Studio (EM simulation software) simulated the two proposed filters in this study. Field distribution of the fundamental mode and second mode is displayed in Fig. 2.

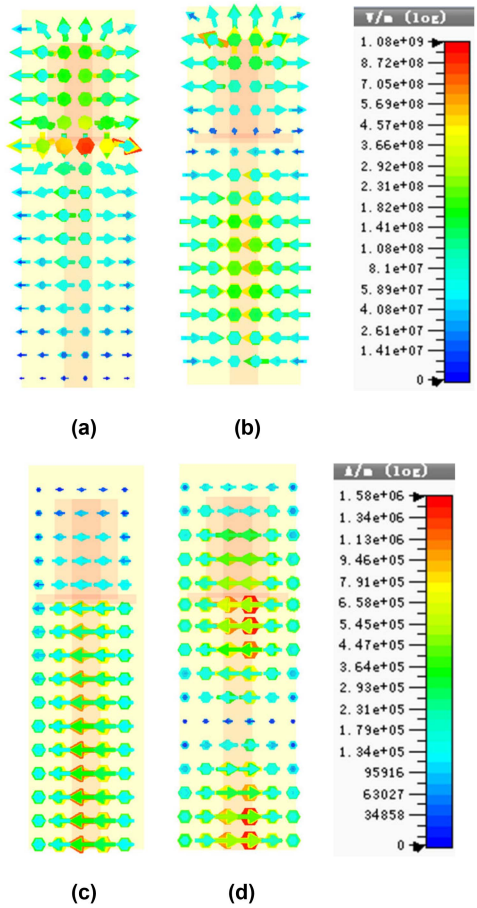

FIGURE 2. (a) E-field of the fundamental mode. (b) E-field of the second mode. (c) B-field of the fundamental mode. (d) B-field of the second mode.

Fig. 2(a)–(d) respectively depict the electric field (E-field) distribution of the fundamental mode, the E-field distribution of the second mode, the magnetic (B-field) distribution of the fundamental mode, and the B-field distribution of the second mode. We can find that with the loading of a disk, the position of the strongest E-field moves down from the top to the loading position at the fundamental mode resonance. On the contrary, the electric field at the loading position is the weakest at the second mode resonance. For B-field, its strength is just the opposite of the electric field. The stronger the electric field is, the weaker the magnetic field is, and vice versa.

The first two resonant frequencies of DLCSIR are employed as the first and second passband center frequencies, namely, f_{res1} and f_{res2}. The resonant frequencies of the first three resonant modes against the dimensions of $\emptyset_2$ and $\emptyset_3$ are shown in Fig. 3(a) and (b). In Fig. 3(a), $\emptyset_3 = \emptyset_1$ is a testing condition, and the aim is to observe the resonance characteristics of coaxial SIR without disk loading. Fig. 3(a) illustrates that the resonant frequencies of the first two modes (f_{res1} and f_{res2}) keep away from each other as $\emptyset_2$ increases. Meanwhile, the frequency of the third resonant mode (f_{res3}) decreases as $\emptyset_2$ increases, especially when $\emptyset_2$ is greater than 8, and f_{res3} decreases sharply. Fig. 3(b) illustrates that the

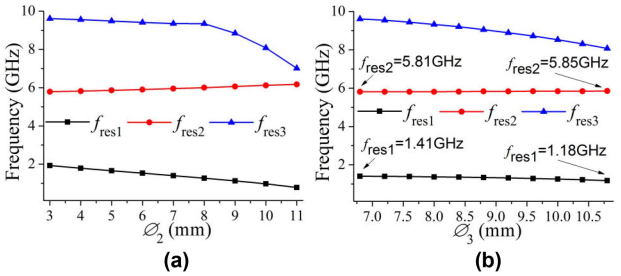

FIGURE 3. (a) Resonant frequencies of the first three modes against $\varnothing_2$, when $\varnothing_3 = \varnothing_1$. (b) Resonant frequencies of the two modes against $\varnothing_2$, when $\varnothing_2 = 6.6$ mm.

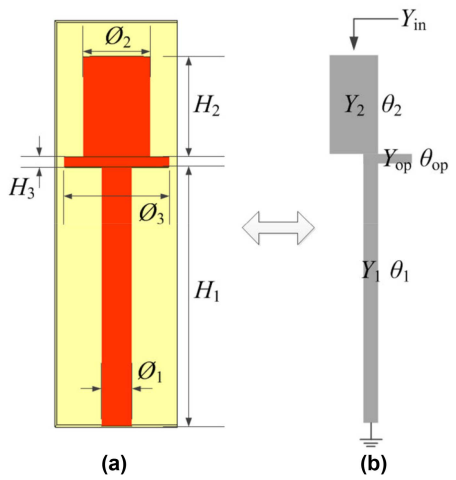

FIGURE 4. (a) Structures of DLCSIR. (b) The transmission line equivalent model stub-loaded quarter-wavelength step impedance resonator.

resonant frequencies of the first and the third modes (f_{res1} and f_{res3}) decrease as $\varnothing_3$ increases, while the resonant frequencies of the second mode are nearly unchanged. The reason is that the electric field at the loading position is the weakest at the second mode resonance, which leads to the loading disk having little effect on DLCSIR at the second mode [23]. Therefore, according to Fig. 3(a) and (b), the conclusion is that the frequency ratio (f_{res2}/f_{res1}) can be further increased based on coaxial SIR by loading a disk.

As shown in Fig. 4, DLCSIR is equivalent to the transmission line model of the stub-loaded quarter-wavelength step impedance resonator [24]. The input admittance of DLCSIR can be obtained by

$$Y_{in} = jY_2 \frac{Y_{op}\tan\theta_{op} - Y_1\cot\theta_1 + Y_2\tan\theta_2}{Y_2 + Y_1\tan\theta_2\cot\theta_1 - Y_{op}\tan\theta_2\tan\theta_{op}} \quad (1)$$

Analytic expressions of resonance condition can be derived by

$$\theta_{2(2)} = \frac{\pi}{2} \; and \; \theta_{1(2)} = \pi \quad \text{at} \quad f = f_2 \quad (2)$$

$$\theta_{2(1)} = \theta_{2(2)}\frac{f_1}{f_2}, \theta_{1(1)} = \theta_{1(2)}\frac{f_1}{f_2} \quad (3)$$

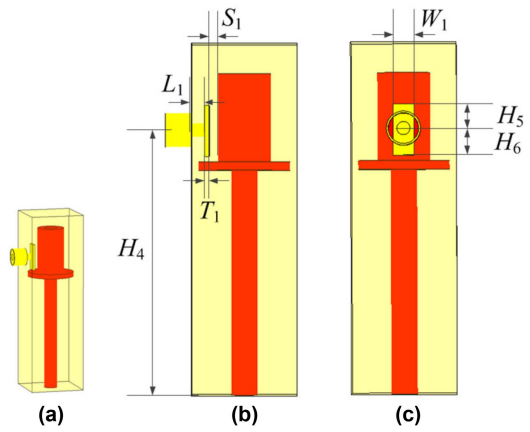

FIGURE 5. Feeding structure (a) Three-dimensional view. (b) Front view. (c) Left side view.

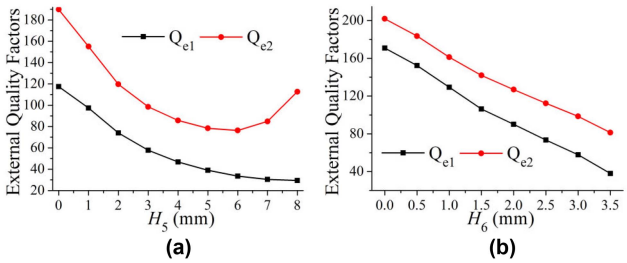

FIGURE 6. (a) The external quality factors of the first two resonant modes against H_5 with fixed $H_6 = 3$ mm. (b) The external quality factors of the first two resonant modes against H_6 with fixed $H_5 = 4$ mm.

$$\theta_{op(1)} = \arctan\left(\frac{Y_1\cot\theta_{1(1)} - Y_2\tan\theta_{2(1)}}{Y_{op}}\right) \quad \text{at} \quad f = f_1 \quad (4)$$

Where f_1 and f_2 are the first two (fundamental mode and second mode) resonant frequencies of the resonator, respectively. $\theta_{1(2)}$ and $\theta_{2(2)}$ denote the electrical lengths at f_2. $\theta_{1(1)}$, $\theta_{2(1)}$, and $\theta_{op(1)}$ are the electrical lengths at f_1. Y_1 and Y_2 represent the admittances of the resonator. According to Eqs. (2) and (4), the conclusion is that $\theta_1 = 2\theta_2$ and the loading stub doesn't affect the resonator at the second resonant mode but have an effect on the first resonant mode. The parameters of DLCSIR H_1, H_2, H_3, $\varnothing_1$, $\varnothing_2$, $\varnothing_3$, f_{res1}, and f_{res2} are related to the parameters of the resonator θ_1, θ_2, Y_{op}, Y_1, Y_2, θ_{op}, f_1, and f_2, respectively. Therefore, the previous conclusion can be changed to $H_1 = 2H_2$, and the loading disk has little effect on DLCSIR at the second resonant mode, but it affects the resonant frequencies of the fundamental mode.

B. FEEDING STRUCTURE AND COUPLING STRUCTURE

As shown in Fig. 5(a)–(c), a simple feeding structure using a rectangular plate is proposed. Fig. 6(a) and (b) show the external quality factors of the first two resonant modes against the dimensions of the rectangular plate (H_5 and H_6). In Fig. 6(a), the external quality factors of the first two resonant modes (Q_{e1} and Q_{e2}) decrease as H_5 increases from 0 mm to 6 mm.

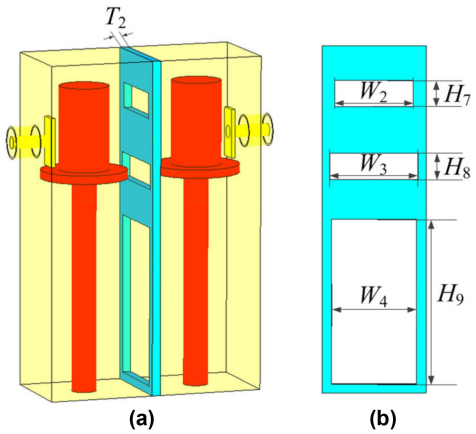

FIGURE 7. Coupling structure (a) Three-dimensional view. (b) Left side view.

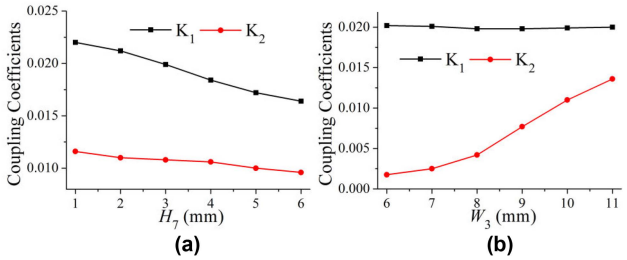

FIGURE 8. (a) The coupling coefficients of the first two modes against H_7. (b) The coupling coefficients of the two modes against W_3.

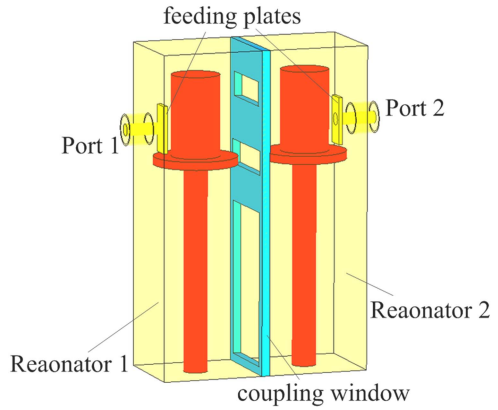

FIGURE 9. Three-dimensional view of the proposed second-order dual-narrowband filter (Filter I).

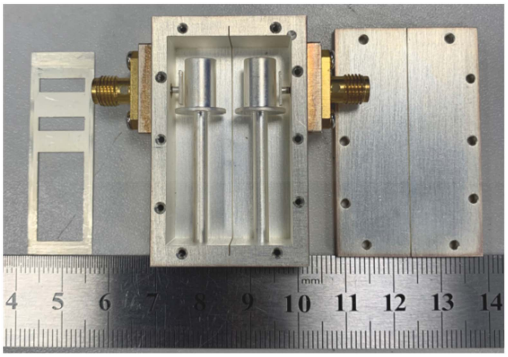

FIGURE 10. Photographs of Filter I.

When H_5 increases from 6 mm to 8 mm, the Q_{e1} remains decreasing, while the Q_{e2} increases. The Q_{e1} and Q_{e2} decrease with the increase of H_6 in Fig. 6(b).

Fig. 7(a) and (b) show the coupling structure with three apertures. The top aperture and the bottom aperture are used to provide electric and magnetic coupling for two coupling coefficients of the first two modes (K_1 and K_2), respectively, and the middle aperture, whose height is facing the loading point is used to control K_2 independent. As shown in Fig. 8(a), K_1 and K_2 decrease when H_7 varies from 1 to 6 mm, and K_1 decreases faster than K_2. By contrast, in Fig. 7(b), when W_3 varies from 6 to 11 mm, K_2 increases, and K_1 is nearly unchanged. The reason is the difference in B-field distributions of the first two modes. The B-field at the loading position is the weakest at the fundamental mode resonance and strongest at the second mode. Therefore, K_1 and K_2 can be achieved by selecting different combinations of H_7 and W_3.

C. FILTER ANALYSIS AND RESULT

A second-order dual-narrowband bandpass filter (Filter I) using DLCSIR is designed and implemented. The two center frequencies of the two passbands are1.2 and 5.8 GHz, and two ripple 0.0432 dB FBWs of 1.2% and 0.6% are selected. The lumped circuit element values of the Chebyshev lowpass prototype filter with ripple 0.0432dB are $g_0 = 1$, $g_1 = 0.6648$, and $g_2 = 0.5445$. The external quality factors (Q_{e1} and Q_{e2}) and coupling coefficients (K_1 and K_2) of the two passbands can be calculated from [25]

$$Q_{e1} = \frac{g_0 g_1}{FBW_1} = 55.4 \quad Q_{e2} = \frac{g_0 g_1}{FBW_2} = 110.8 \tag{5}$$

$$K_1 = \frac{FBW_1}{\sqrt{g_1 g_2}} = 0.02 \quad K_2 = \frac{FBW_2}{\sqrt{g_1 g_2}} = 0.01 \tag{6}$$

According to Fig. 6, Q_{e1} and Q_{e2} can be realized by H_5 and H_6. By contrast, according to Fig. 8, K_1 and K_2 can be achieved by H_7 and W_3, respectively. The configuration of the proposed second-order dual-narrowband filter, named Filter I, is shown in Fig. 9. The circuit is symmetric about the central plane of the coupling window. The fabricated filter by adopting a silver-plated copper cavity is provided in Fig. 10. The physical dimensions of the fabricated prototype of Filter I are shown in Table 1. The internal dimensions of this filter I are 12 mm × 25 mm × 40 mm, and in the two passbands, the unloaded Q values are respectively 1900 and 3470.

Fig. 11 shows the filter along with the simulated and test results. The measured inband insertion losses are approximate 0.43 and 0.40 dB at 1.2 and 5.8 GHz, respectively. The measured inband return losses are below 14 and 28 dB, and the simulated inband return losses are below 21 and 24 dB. The slight discrepancy is primarily caused by an extra soldering width between the Small-A-Type (SMA) connectors and the

TABLE 1. Dimensions of Fabricated Prototype of Filter I

DLCSIRs	Feeding plates	Coupling window	Cavity
H_1: 25.6 mm	S_1: 0.67 mm	T_2: 0.2 mm	w: 12 mm
H_2: 9.9 mm	L_1: 1.53 mm	W_2: 10 mm	h: 40 mm
H_3: 1 mm	T_1: 0.5 mm	W_3: 10.2 mm	
$Ø_1$: 3 mm	W_1: 2.4 mm	W_4: 9.8 mm	
$Ø_2$: 6.6 mm	H_4: 30.2 mm	H_7: 3 mm	
$Ø_3$: 10.4 mm	H_5:3.8 mm	H_8: 3 mm	
	H_6: 3 mm	H_9: 19 mm	

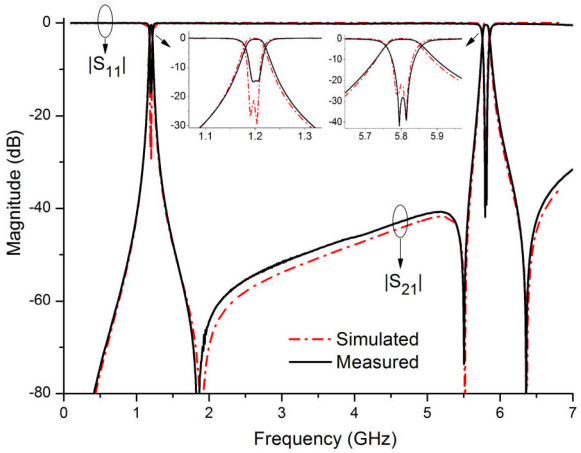

FIGURE 11. Simulated and measured results of Filter I.

feeding lines. Besides, the S-parameters of test results and simulation results are consistent regarding the center frequencies, the transmission zeros, and fractional bandwidth.

III. DUAL-WIDEBAND FILTER DESIGN

A. RCSIR ANALYSIS

To achieve dual-wideband characteristics with a large frequency ratio, RCSIR is proposed. Compared with the DLCSIR mentioned above, to achieve strong coupling, the cylindrical structure is changed to a rectangular structure, and the loaded disk is removed. The configuration of RCSIR is shown in Fig. 12. This resonator is formed on a cuboid cavity with the length and width both are parameters w_1 and w_2, and the height is parameter h. The bottom sidewall of the cavity is embedded with a rectangular stepped impedance line, which is not placed in the center of the cavity for realizing independent control of resonant frequencies and strong coupling. AA' and BB' are the symmetry planes of Fig. 12(a) and (b), and the corresponding offsets are p and q, respectively. The value of gap S_1 is minimal for equivalent strong coupling between resonators. The Field distribution of the fundamental mode and second mode of RCSIR is displayed in Fig. 13. Fig. 13(a)–(d) respectively show the E-field distribution of the fundamental

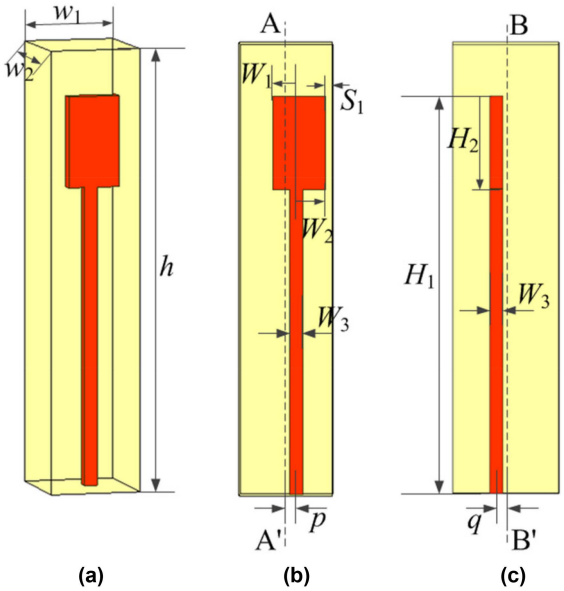

FIGURE 12. Proposed DLCSIR. (a) Three-dimensional view. (b) Front view. (c) Left side view.

mode, E-field distribution of the second mode, B-field distribution of the fundamental mode, and B-field distribution of the second mode. Compared with the E-field of the two modes, the E-field of the fundamental mode is stronger than that of the second mode in the upper left region of Fig. 13(a) and (b), and even the reverse electric field appears at the second mode when the height decreases. Compared with the B-field of the two modes, the reverse magnetic field appears at the second mode in the bottom region of Fig. 13(d).

The first two resonant frequencies of RCSIR are used as the first and second passband frequencies, namely, f_{res1} and f_{res2}. The resonant frequencies of the first three resonant modes against the dimensions of H_2 and W_1 are shown in Fig. 14(a) and (b). In Fig. 14(a), the resonant frequencies of the first two modes (f_{res1} and f_{res2}) keep away as H_2 increases due to the reverse electric field at the second mode. Fig. 14(b) illustrates that the resonant frequencies of the first and the third modes (f_{res1} and f_{res3}) decrease as W_1 increases, while the resonant frequencies of the second mode are nearly unchanged. The reason is that the E-field of the fundamental mode is much stronger than that of the second mode in the upper left region of the Fig. 13(a) and (c). Therefore, according to Fig. 14(a) and (b), the desired f_{res1} and f_{res2} can be achieved.

B. FEEDING STRUCTURE AND COUPLING STRUCTURE

As shown in Fig. 15(a), a simple tapping feeding structure is employed. Fig. 15(b) shows the external quality factors of the first two resonant modes against the dimensions of the tapping position, H_t. The external quality factors of the first two resonant modes (Q_{e1} and Q_{e2}) decrease as H_t increases from 5 mm to 25 mm. When H_t increases from 25 mm to 40 mm, the Q_{e1} remains decreasing, while the Q_{e2} increases.

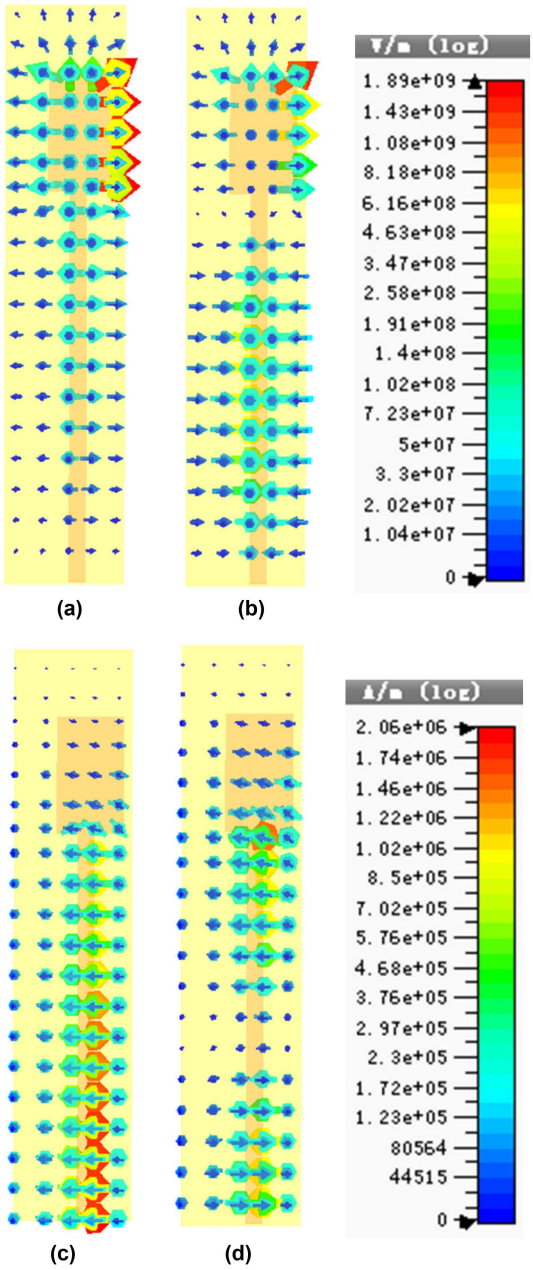

FIGURE 13. (a) E-field of the fundamental mode. (b) E-field of the second mode. (c) B-field of the fundamental mode. (d) B-field of the second mode.

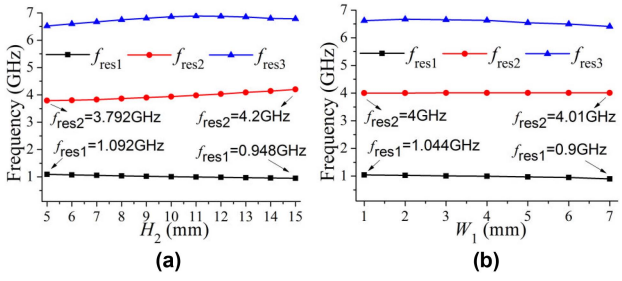

FIGURE 14. (a) Resonant frequencies of the first three modes against H_2. (b) Resonant frequencies of the three modes against W_1.

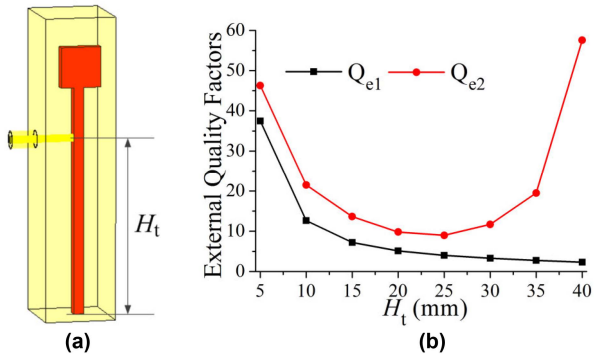

FIGURE 15. (a) Feeding structure. (b) The external quality factors of the first two resonant modes against H_t.

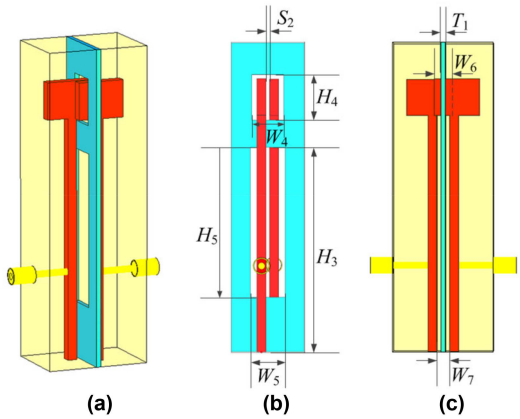

FIGURE 16. Coupling structure. (a) Three-dimensional view. (b) Left side view. (c) Front view.

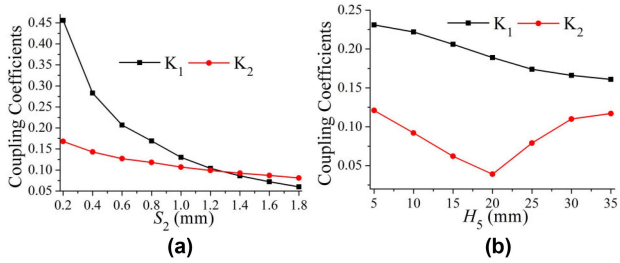

FIGURE 17. (a) The coupling coefficients of the first two modes against S_2. (b) The coupling coefficients of the two modes against H_5.

The ranges of Q_{e1} and Q_{e2} are relatively large due to the wide range of H_t.

Fig. 16(a)–(c) show the coupling structure, which consists of two apertures. The top aperture provides strong electric coupling for two coupling coefficients of the first two modes (K_1 and K_2). In order to realize strong coupling, the two rectangular stepped impedance lines pass through the top aperture, and the strong coupling coefficients are mainly decided by S_2 and W_6. The bottom aperture is used to fine-tune K_1 and K_2. As shown in Fig. 17(a), K_1 and K_2 decrease when

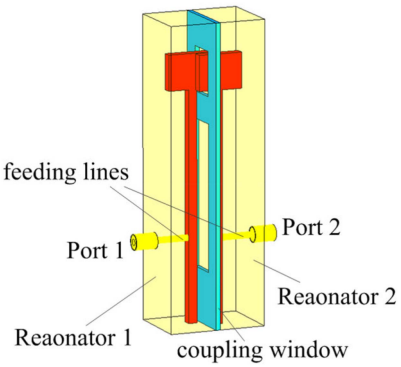

FIGURE 18. Three-dimensional view of the proposed second-order dual-wideband filter (Filter II).

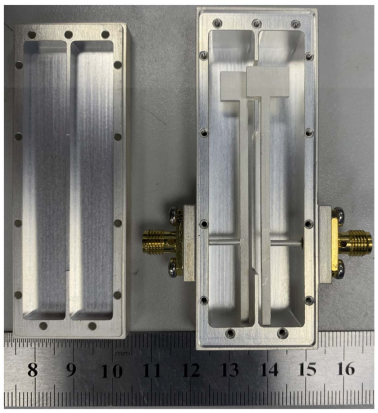

FIGURE 19. Photographs of Filter II.

S_2 increases from 0.2 to 1.8 mm, and K_1 decreases faster than K_2. The large values of K_1 and K_2 also verify the strong coupling characteristic. In Fig. 17(b), K_1 and K_2 decrease as H_5 increases from 5 mm to 20 mm. When H_5 increases from 20 mm to 35 mm, K_1 decreases, while the K_2 increases due to the reverse E-field at the second mode. Therefore, K_1 and K_2 can be realized by selecting different combinations of S_2 and H_5.

C. FILTER ANALYSIS AND RESULT

A second-order dual-wideband bandpass filter (Filter II) using RCSIR is designed and implemented. The two center frequencies of the two passbands are 1 and 4 GHz, and two ripple 0.0432 dB FBWs of 9% and 7% are selected. The lumped circuit element values of the Chebyshev lowpass prototype filter with ripple 0.0432 dB are $g_0 = 1$, $g_1 = 0.6648$, and $g_2 = 0.5445$. The external quality factors (Q_{e1} and Q_{e2}) and coupling coefficients (K_1 and K_2) of the two passbands can be calculated as:

$$Q_{e1} = \frac{g_0 g_1}{FBW_1} = 7.39 \quad Q_{e2} = \frac{g_0 g_1}{FBW_2} = 9.5 \tag{7}$$

$$K_1 = \frac{FBW_1}{\sqrt{g_1 g_2}} = 0.15 \quad K_2 = \frac{FBW_2}{\sqrt{g_1 g_2}} = 0.117 \tag{8}$$

According to Fig. 15, Q_{e1} and Q_{e2} are decided by H_t. By contrast, according to Fig. 17, K_1 and K_2 can be achieved by S_2 and H_5. The configuration of the proposed second-order dual-wideband filter, named Filter II, is shown in Fig. 18. The circuit is symmetric about the central line of the coupling windows. The fabricated filter by adopting a silver-plated copper cavity is provided in Fig. 19. The physical dimensions of the fabricated prototype of Filter II are given in Table 2. The internal dimensions of Filter II are 22 mm × 16 mm × 68 mm, and in the two passbands, the unloaded Q values are respectively 740 and 1190.

The measured S-parameters are compared with the simulated ones in Fig. 20. The measured minimal insertion losses are approximate 0.39 and 0.16 dB at 0.98 and 4.06 GHz, respectively. In contrast, the measured return losses are below 14 and 24 dB. Finally, Table 3 compares the two proposed filters with several reported cavity dual-band filters, which show the advantages of this work in terms of large frequency ratios and miniaturized size.

TABLE 2. Dimensions of Fabricated Prototype of Filter II

RCSIRs	Feeding lines	Coupling window	Cavity
H_1: 60 mm	H_t: 19 mm	T_1: 1 mm	w_1: 10.5 mm
H_2: 7.9 mm		S_2: 0.8 mm	w_2: 16 mm
W_1: 5.6 mm		W_4: 7 mm	h: 68 mm
W_2: 4.4 mm		W_5: 7.6 mm	
W_3: 2 mm		W_6: 4 mm	
p: 3.35 mm		W_7: 2.8 mm	
q: 1.4 mm		H_3: 45 mm	
		H_4: 8.9 mm	
		H_5: 33 mm	

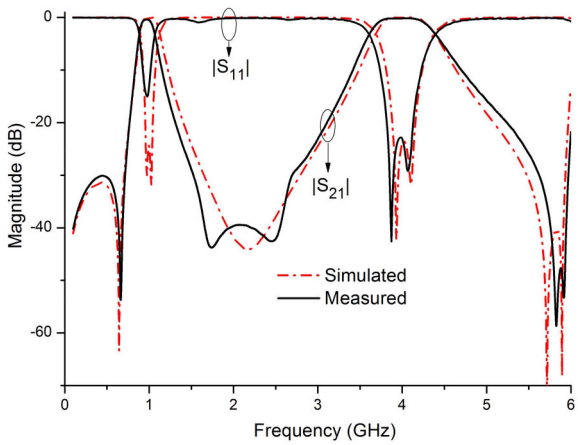

FIGURE 20. Simulated and measured results of Filter II.

TABLE 3. Comparisons With Other Reported Cavity DB-BPFs

Ref.	CF of 1st/2nd Passband (GHz)	Order	Insertion Loss (dB)	Types of Cavities	FBW of 3dB	Circuit Size of One Order (mm×mm×mm) (λg×λg×λg)
[5] Filter I	5/5.6	2	0.25/0.27	Dielectric loaded	1%/ 1%	(26.6×26.6×20.6) (0.44×0.44×0.34)
[5] Filter II	2.6/3.5	3	0.45/0.4	Dielectric loaded	0.7%/ 1.1%	-
[6]	4.25/4.55	3	1.3/1.15	Dielectric loaded	1.5%/ 1.5%	(15×26×19) (0.21×0.37×0.27)
[8]	0.43/0.91	2	2.1/3.1	Helical	1.85% /0.77 %	(24×32×42) (0.03×0.04×0.05)
[11]	11.06/ 11.59	8	0.4/0.4	Waveguide	1.8%/ 1.7%	(22.4×24.8×17.3) (0.82×0.91×0.64)
[12]	5/7.5	4	1.21/1.71	Waveguide	5%/ 5%	(43.1×43.1×46.8) (0.72×0.72×0.78)
[19]	0.9/1.8	3	1.1/1.9	Coaxial	1%/ 0.6%	(50×50×111.3) (0.15×0.15×0.33)
[22]	0.9/1.8	3	0.22/0.25	Coaxial	30%/ 15%	(50×67×162) (0.15×0.2×0.49)
This work Filter I	1.2/5.8	2	0.43/0.40	Modified coaxial	3.7%/ 1.7%	(12×12×40) (0.07×0.07×0.24)
This work Filter II	1/4	2	0.39/0.16	Modified coaxial	19%/ 20%	(10.5×16×68) (0.03×0.05×0.23)

IV. CONCLUSION

Two types of dual-narrowband/wideband filters have been proposed using modified coaxial cavities with large frequency ratios. DLCSIRs are adopted to realize the dual-narrowband filter. The frequency ratios of DLCSIR can be controlled by the impedance ratio and loading disk. In contrast, RCSIRs are utilized to achieve the dual-wideband filter. Two rectangular stepped impedance lines pass through the top aperture, which provides a strong coupling. Finally, the two proposed filters are designed, fabricated, and tested with good results. The proposed techniques are potentially applicable to multi-band systems with large frequency ratios.

REFERENCES

[1] S. Y. Zheng, Z. L. Su, Y. M. Pan, Z. Qamar, and D. Ho, "New dual-/tri-band bandpass filters and diplexer with large frequency ratio," *IEEE Trans. Microw. Theory Techn.*, vol. 66, no. 6, pp. 2978–2992, Jun. 2018.

[2] Y. Su, Y. Fan, X. Q. Lin, and K. Wu, "Single-layer mode composite coplanar waveguide dual-band filter with large frequency ratio," *IEEE Trans. Microw. Theory Techn.*, vol. 68, no. 6, pp. 2320–2330, Jun. 2020.

[3] W. S. Tang, S. Zheng, Y. Pan, and H. Liu, "A frequency independently tunable dual-band bandpass filter with large frequency ratio and ultra-wide stopband," *IEEE Trans. Ind. Electron.*, early access, Mar. 29, 2022, doi: 10.1109/TIE.2022.3161816.

[4] J.-X. Chen, J. Li, and J. Shi, "Miniaturized dual-band differential filter using dual-mode dielectric resonator," *IEEE Microw. Wireless Compon. Lett.*, vol. 28, no. 8, pp. 657–659, Aug. 2018.

[5] R. Zhang and R. R. Mansour, "Dual-band dielectric-resonator filters," *IEEE Trans. Microw. Theory Techn.*, vol. 57, no. 7, pp. 1760–1766, Jul. 2009.

[6] V. Nocella, L. Pelliccia, C. Tomassoni, and R. Sorrentino, "Miniaturized dual-band waveguide filter using TM dielectric-loaded dual-mode cavities," *IEEE Microw. Wireless Compon. Lett.*, vol. 26, no. 5, pp. 310–312, May 2016.

[7] A. Widaa and M. Höft, "Miniaturized dual-band dual-mode TM-mode dielectric filter in planar configuration," *IEEE J. Microwaves*, vol. 2, no. 2, pp. 326–336, Apr. 2022.

[8] Q.-X. Chu and Z.-C. Zhang, "Dual-band helical filters based on nonuniform pitch helical resonators," *IEEE Trans. Microw. Theory Techn.*, vol. 65, no. 8, pp. 2886–2892, Aug. 2017.

[9] S. Amari and M. Bekheit, "A new class of dual-mode dual-band waveguide filters," *IEEE Trans. Microw. Theory Techn.*, vol. 56, no. 8, pp. 1938–1944, Aug. 2008.

[10] L. Zhu, R. R. Mansour, and M. Yu, "Compact triple-band bandpass filters using rectangular waveguide resonators," in *Proc. IEEE MTT-S Int. Microw. Symp.*, 2016, pp. 1–3.

[11] L. Zhu, R. R. Mansour, and M. Yu, "Compact waveguide dual-band filters and diplexers," *IEEE Trans. Microw. Theory Techn.*, vol. 65, no. 5, pp. 1525–1533, May 2017.

[12] U. Naeem, A. Perigaud, and S. Bila, "Dual-mode dual-band bandpass cavity filters with widely separated passbands," *IEEE Trans. Microw. Theory Techn.*, vol. 65, no. 8, pp. 2681–2686, Aug. 2017.

[13] L. Zhu, R. R. Mansour, and M. Yu, "Triple-band cavity bandpass filters," *IEEE Trans. Microw. Theory Techn.*, vol. 66, no. 9, pp. 4057–4069, Sep. 2018.

[14] S.-W. Wong, Z.-C. Guo, J.-Y. Lin, L. Zhu, and Q. Zhang, "Triple-mode and triple-band cavity bandpass filter on triplet topology with controllable transmission zeros," *IEEE Access*, vol. 6, pp. 29452–29459, 2018.

[15] Z.-C. Guo, S.-W. Wong, and L. Zhu, "Triple-passband cavity filters with high selectivity under operation of triple modes," *IEEE Trans. Compon., Packag., Manuf. Technol.*, vol. 9, no. 7, pp. 1337–1344, Jul. 2019.

[16] G. Macchiarella and S. Tamiazzo, "Design techniques for dual-passband filters," *IEEE Trans. Microw. Theory Techn.*, vol. 53, no. 11, pp. 3265–3271, Nov. 2005.

[17] X. G. Liu, L. P. B. Katehi, and D. Peroulis, "Novel dual-band microwave filter using dual-capacitively-loaded cavity resonators," *IEEE Microw. Wireless Compon. Lett.*, vol. 20, no. 11, pp. 610–612, Nov. 2010.

[18] J. A. Ruiz-Cruz, M. M. Fahmi, and R. R. Mansour, "Triple-conductor combline resonators for dual-band filters with enhanced guard-band selectivity," *IEEE Trans. Microw. Theory Techn.*, vol. 60, no. 12, pp. 3969–3979, Dec. 2012.

[19] F.-C. Chen, J.-M. Qiu, S.-W. Wong, and Q.-X. Chu, "Dual-band coaxial cavity bandpass filter with helical feeding structure and mixed coupling," *IEEE Microw. Wireless Compon. Lett.*, vol. 25, no. 1, pp. 31–33, Jan. 2015.

[20] Y. Wu, R. Gajaweera, and J. Everard, "Dual-band bandpass filter using coaxial stepped impedance resonators," in *Proc. Int. Conf. Students Appl. Eng.*, Oct. 2016, pp. 181–185.

[21] E. Doumanis, L. Guan, G. Goussetis, and D. Ferling, "Dual-band bandpass double ground plane coaxial resonators and filters," *IEEE Trans. Microw. Theory Techn.*, vol. 66, no. 8, pp. 3828–3835, Aug. 2018.

[22] Y. Xie, F.-C. Chen, Q.-X. Chu, and Q. Xue, "Dual-band coaxial filter and diplexer using stub-loaded resonators," *IEEE Trans. Microw. Theory Techn.*, vol. 68, no. 7, pp. 2691–2700, Jul. 2020.

[23] Z.-C. Zhang, Q.-X. Chu, and F.-C. Chen, "Compact dual-band bandpass filters using open-/short-circuited stub-loaded λ/4 resonators," *IEEE Microw. Wireless Compon. Lett.*, vol. 25, no. 10, pp. 657–659, Oct. 2015.

[24] Z.-C. Zhang, Q.-X. Chu, and F. C. Chen, "Novel quad-band filter with high frequency ratio and controllable bandwidths using SLHSIRs and SLQSIRs," *Microw. Opt. Technol. Lett.*, vol. 56, no. 12, pp. 2845–2848, Dec. 2014.

[25] J.-S. Hong and M. J. Lancaster, *Microstrip Filters for RF/Microwave Applications*. New York, NY, USA: Wiley, 2001.

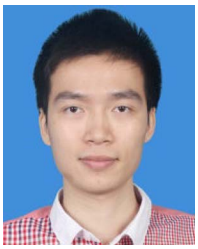

ZHI-CHONG ZHANG (Member, IEEE) was born in Ji'an, Jiangxi, China. He received the B.S. degree in communication engineering from Nanchang University, Nanchang, China, in 2008, the M.E. degree in communication and information system from the East China of Jiaotong University, Nanchang, China, in 2012, and the Ph.D. degree in electromagnetic fields and microwave technology from the South China University of Technology, Guangzhou, China, in 2015. Since 2020, he has been an Associate Professor with the School of Electronic and Information Engineering, Jinggangshan University, Ji'an, China. His research interests include the design of microwave filters and associated RF modules for microwave and millimeter-wave applications.

HONG-JI LI was born in Guangdong, China. He is currently working toward the B.E. degree with the College of Electronics and Information Engineering, Shenzhen University, Shenzhen, China. His research interests include microwave filter, antenna, and cavity components design.

XU-ZHOU YU (Student Member, IEEE) received the B.E. degree from the School of Electronic and Information Engineering, Tianjin University, Tianjin, China, in 2019. He is currently working toward the master's degree with the College of Electronics and Information Engineering, Shenzhen University, Shenzhen, China. His research interests include microwave cavity circuit design.

YEJUN HE (Senior Member, IEEE) received the Ph.D. degree in information and communication engineering from Huazhong University of Science and Technology, Wuhan, China, in 2005. From 2005 to 2006, he was a Research Associate with the Department of Electronic and Information Engineering, The Hong Kong Polytechnic University, Hong Kong. From 2006 to 2007, he was a Research Associate with the Department of Electronic Engineering, Faculty of Engineering, The Chinese University of Hong Kong, Hong Kong. In 2012, he was a Visiting Professor with the Department of Electrical and Computer Engineering, University of Waterloo, Waterloo, ON, Canada. From 2013 to 2015, he was an Advanced Visiting Scholar (Visiting Professor) with the School of Electrical and Computer Engineering, Georgia Institute of Technology, Atlanta, GA, USA. Since 2011, he has been a Full Professor with the College of Electronics and Information Engineering, Shenzhen University, Shenzhen, China, where he is currently the Director of the Guangdong Engineering Research Center of Base Station Antennas and Propagation and the Director of the Shenzhen Key Laboratory of Antennas and Propagation, Shenzhen, China. He was selected as a Pengcheng Scholar Distinguished Professor, Shenzhen, and Minjiang Scholar Chair Professor of Fujian Province. He has authored or coauthored more than 230 referred journal and conference papers and seven books (chapters) and holds about 20 patents. His research interests include wireless communications, antennas, and radio frequency. He was the recipient of the Shenzhen Science and Technology Progress Award and Guangdong Provincial Science and Technology Progress Award in 2017 and 2018, respectively. He was also the recipient of the Shenzhen Overseas High-Caliber Personnel Level B (Peacock Plan Award B) and Shenzhen High-Level Professional Talent (Local Leading Talent). He was a reviewer of various journals, and also was the Technical Program Committee member or the Session Chair of various conferences. He is the Principal Investigator for more than 30 current or finished research projects, including the National Natural Science Foundation of China, Science and Technology Program of Guangdong Province, and Science and Technology Program of Shenzhen City. He is a Fellow of IET and a Senior Member of the China Institute of Communications and the China Institute of Electronics. He is an Associate Editor for IEEE TRANSACTIONS ON ANTENNAS AND PROPAGATION, *IEEE Antennas and Propagation Magazine*, IEEE NETWORK, *International Journal of Communication Systems*, *China Communications*, *ZTE Communications*, and *Wireless Communications and Mobile Computing*.

SAI-WAI WONG (Senior Member, IEEE) received the B.S degree in electronic engineering from the Hong Kong University of Science and Technology, Hong Kong, in 2003, and the M.Sc. and Ph.D. degrees in communication engineering from Nanyang Technological University, Singapore, in 2006 and 2009, respectively. From July 2003 to July 2005, he was leading the Engineering Department in mainland of China with two Hong Kong manufacturing companies. From 2009 to 2010, he was a Research Fellow with the Institute for Infocomm Research, Singapore. Since 2010, he has been an Associate Professor and then a Full Professor with the School of Electronic and Information Engineering, South China University of Technology, Guangzhou, China. In 2016, he was a Visiting Professor with the City University of Hong Kong. In 2017, he was a Visiting Professor with the University of Macau, Zhuhai, China. Since 2017, he has been a Full Professor with the College of Electronics and Information Engineering, Shenzhen University, Shenzhen, China. His research interests include RF/microwave circuit and antenna design. Dr. Wong was the recipient of the New Century Excellent Talents in University (NCET) Award in 2013 and the Shenzhen Overseas High-Caliber Personnel Level C in 2018. He is also a reviewer of several top-tier journals.